Vehicle System Dynamics, Vol. 55, Issue 11, 2017, pp. 1665-1685
DOI:10.1080/00423114.2017.1318212

To appear in *Vehicle System Dynamics*
Vol. 00, No. 00, Month 20XX, 1–21

Wheel Slip Control with Torque Blending using Real Time Model Predictive Control

M. Sofian Basrah*, Efstathios Siampis, Efstathios Velenis, Dongpu Cao and Stefano Longo
Advanced Vehicle Engineering Centre, School of Aerospace, Transport and Manufacturing, Cranfield University, Cranfield, UK

(*Received 00 Month 20XX; accepted 00 Month 20XX*)

Modern Hybrid Electric Vehicles employ electric braking to recuperate energy during deceleration. However, currently Anti-lock Braking System (ABS) functionality is delivered solely by friction brakes. Hence regenerative braking is typically deactivated at a low deceleration threshold in case high slip develops at the wheels and ABS activation is required. If blending of friction and electric braking can be achieved during ABS events, there would be no need to impose conservative thresholds for deactivation of regenerative braking and the recuperation capacity of the vehicle would increase significantly. In addition, electric actuators are typically significantly faster responding and would deliver better control of wheel slip than friction brakes. In this work we present a control strategy for ABS on a fully electric vehicle with each wheel independently driven by an electric machine and friction brake independently applied at each wheel. In particular we develop linear and nonlinear model predictive control strategies for optimal performance and enforcement of critical control and state constraints. The capability for real time implementation of these controllers is assessed and their performance is validated in high fidelity simulation.

Keywords: hybrid electric vehicle; real time; nonlinear model predictive control; MPC; ABS; slip control; torque allocation

Notation

μ	Tyre-road friction coefficient
δ	Steering wheel angle
$\dot{\psi}$	Vehicle yaw rate
ω	Wheel rotational speed
a_x	Vehicle longitudinal acceleration at its centre of mass
F_x, F_z	Longitudinal and normal tyre force
g	Constant of gravitational acceleration
i, j	Subscripts $i = F, R$ (front, rear), $j = L, R$ (left, right)
m	Mass of the vehicle
R_w	Wheel radius
s_x	Longitudinal wheel slip

*Corresponding author. Email: s.s.basrah@cranfield.ac.uk

Published by Taylor & Francis. This is the Author Accepted Manuscript issued with:
Creative Commons Attribution Non-Commercial License (CC:BY:NC 4.0).
The final published version (version of record) is available online at DOI:10.1080/00423114.2017.1318212
Please refer to any applicable publisher terms of use.

B	Pacejka's Magic Formula stiffness factor
C	Pacejka's Magic Formula shape factor
D	Pacejka's Magic Formula peak value
J_w	Wheel moment of inertia of each wheel about its axis of rotation
N	Horizon
N_p	Prediction horizon
N_u	Control horizon
T_e	EM Torque
T_h	Hydraulic braking torque
T_s	Sampling time
T_{sim}	Simulation time
V_x	Vehicle velocity

1. Introduction

Vehicle electrification is part of a major initiative by automotive manufacturers towards a solution to emissions and global warming issues [1]. The diminishment of the fossil fuel resources is another major contribution to the rapid growth of hybrid electric vehicle technology [2]. Vehicle electrification entails the incorporation of electric machines (EM) and energy storage in the vehicle's powertrain. The existence of the new actuator creates the opportunity not only to increase energy efficiency but to enhance the performance of the safety aspect of the vehicle [3]. Anti-lock braking system (ABS) is an important feature of active vehicle safety to ensure vehicle stability and steerability when the drivers attempt to stop the vehicle during emergency braking. The ABS controls the braking force accordingly when the system identifies incipient wheel lock [4]. The driver will be unable to steer the vehicle as it continues to slide if the front wheels are locked, while the vehicle is prone to spin out and losing control if the rear wheels lock. In addition, brake stopping distance is significantly longer if the wheels are locked during braking in most road surfaces [5]. Regenerative braking can be deployed to support hydraulic friction braking system during braking events to recuperate energy for future use and also during emergency situations, such as to avoid wheel locking. Currently, only conservative strategies have been applied for the deployment of EM during braking, which is disabled if any risk of emergency situation emerges [3, 6, 7].

This work concentrates on enabling the integration of the slip control and torque blending between the braking actuators, namely the hydraulic friction brake (HFB) and regenerative braking systems. The main motivation is to allow for a wider window of regenerative braking activation during high decelerations or emergency braking. Additionally, the distinct advantage of using an electric motor such that accurate and fast control can be applied in improving the slip control operation. Electric machines have limited torque range for braking but have very quick and precise response, and the applied torque can be measured easily [8]. On the other hand, HFB is capable of delivering high retarding torque but is limited by high delay of response [8, 9]. With the combination of the two actuators, ABS performance can be improved and the energy regeneration can have a wider activation window to increase efficiency.

Novel strategies to combine hydraulic and regenerative braking during low wheel slip braking have been reported in [16, 17]. However, the strategies only consider normal braking conditions when there is low risk of wheel locking. On the other hand, torque blending for slip control is a fairly new research area and several articles report torque allocation algorithms using rule-based methods [18, 19]. A brake torque allocation strategy using

a static control allocation or daisy chain method is proposed in [20]. A clear advantage of this approach is the low computational effort for online implementation. Article [9] proposes a torque allocation strategy using optimization methods which consider the two brake actuators dynamics. The disadvantage lies with decoupling of the slip controller and the torque blending algorithm, which requires the calculation of the required total braking torque and the actuators braking torque independently. The proposed approach achieves robustness in wheel slip tracking in the presence of tyre-road friction variations by incorporating an adaptive slip control algorithm. A linear Model Predictive Control (MPC) method is proposed for the torque allocation to work along with a linear slip controller in [21]. This approach still requires an independent slip control algorithm to determine commanded ABS torque before the allocation procedure can take place. A combined slip control and torque allocation algorithm using linear MPC is presented in [22]. The authors demonstrate the enhanced performance of the controller compared to cascaded control approaches, as in [9] and [21]. The MPC controller of [22] uses a low order internal model of slip dynamics, which is linearised with respect to the desired equilibrium condition, assuming slowly varying speed when compared to wheel slip variations. An interesting discussion on stability and robustness of the linear MPC scheme for slip control is presented in [22], considering, however, the unconstrained problem. In [23] a slip control using nonlinear MPC for EV using in-wheel motor (IWM) is proposed. However, there is no indication of real time implementation and no brake torque blending consideration. Furthermore, results shown indicate the wheel slip achieved is much smaller than the desired slip.

In [24] the authors propose a Nonlinear Model Predictive Control (NMPC) approach for integrated slip control and torque blending incorporating important nonlinearities and constraints in the optimisation problem. In this paper we extend the results of [24] to include wheel normal force and vehicle speed estimation in the implementation of the controller. Furthermore, we present the development of a linear MPC controller for the combined slip control and actuators blending problem for comparison against the nonlinear approach. In contrast to [22] we consider update of the linear model with regards to the current operating condition as opposed to a linearisation with respect to a constant target. We also use torque rate, instead of torque, as the input variable to eliminate the need for a reference torque value. In addition we implement the controller in high fidelity simulation considering scenarios involving combined longitudinal and lateral vehicle dynamics, as opposed to most ABS design papers which mainly concentrate on longitudinal dynamics [10–14]. We discuss the capability to implement both strategies in real time, and present a case study of the robustness of the controllers against critical uncertainties in the tyre-road friction.

In the section following this introduction we present modelling of the system dynamics and actuators. In the next section we present the proposed nonlinear and linear MPC strategies followed by vehicle speed and vertical tyre force estimation. A high fidelity model implementation is introduced in the following section followed by discussions of the simulations results. Robustness against uncertainty in the available tyre-road adhesion is presented and finally conclusions are summarised.

2. Modelling

In this section we present the vehicle and tyre models used to construct the proposed MPC strategies. The equations are similar to the one reported in [15]. In addition the braking actuator dynamics are introduced similar to [9].

2.1. *Single-wheel Model*

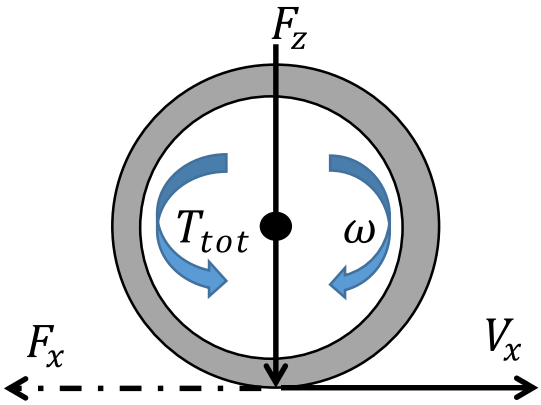

Figure 1. Single-wheel model.

A single-wheel model is used as the internal MPC model. Assume that the continuous-time model is

$$\dot{V}_x = \frac{F_x}{m}, \tag{1}$$

$$\dot{\omega} = \frac{T_{tot} - F_x R_w}{J_w}, \tag{2}$$

$$T_{tot} = T_e + T_h, \tag{3}$$

with V_x the wheel's forward velocity, ω the angular wheel speed, F_x the tyre's longitudinal force, T_{tot} the total torque applied on the wheel and R_w, J_w and m the wheel's radius, moment of inertia and quarter vehicle mass respectively. For our blending strategy, the T_{tot} is the summation of the torque from the electric motor T_e and the torque from the hydraulic brake T_h.

In the above model, F_x is set as a function of longitudinal slip, s_x through a simplified version of Pacejka's Magic Formula (MF) [25]:

$$s_x = \frac{\omega R_w - V_x}{V_x}, \tag{4}$$

$$F_x = F_z D \sin(C \text{atan}(B s_x)), \tag{5}$$

where B, C and D are the MF's factors and F_z the vertical force on the tyre. The wheel and tyre parameters used in this paper can be found in Table 1. We neglect the lateral motion of the vehicle and concentrate on simplified longitudinal motion of the vehicle.

Table 1. Vehicle and tyre parameters.

Parameter		Value
wheel moment of inertia	Jw (kgm^2)	1.04
wheel radius	R_w (m)	0.3
MF's stiffness factor	B	7
MF's shape factor	C	1.6
MF's peak factor	D	1, 0.3

2.2. *Actuator Dynamics*

There are two braking actuators implemented in this work; the hydraulic braking and regenerative braking actuators. Similar to [9, 20] we assume that a brake-by-wire system is used in a way which delivers continuous braking torque instead of the conventional discrete brake pressure control [26]. The response of the brake torque generated by the EM is significantly faster than the one from the hydraulic brake-by-wire system [27]. A first order delay is adopted to represent actuator dynamics for both the hydraulic brakes and the EM in our simulation studies similar to [9]

$$\frac{T_e}{T_e^*} = \frac{1}{\tau_e s + 1} \tag{6}$$

$$\frac{T_h}{T_h^*} = \frac{1}{\tau_h s + 1} \tag{7}$$

where T_e^* the EM reference torque, T_h^* the reference hydraulic brake torque, τ_e and τ_h the time constant for the delay for EM and hydraulic brake respectively. In this work the time constant used for EM and hydraulic brake is set to 1.5ms and 16ms respectively. Although the EM has faster torque response, the retarding torque application is limited in range and generally determined by the battery state of charge, motor speed and operating temperature [3]. On the other hand, the hydraulic braking system can deliver high torque but at slower rate. Then the torque limits are

$$T_e^{min} \leq T_e \leq T_e^{max}, \qquad T_h^{min} \leq T_h \leq T_h^{max}, \tag{8}$$

where

$$T_e^{min} = -750Nm, \qquad T_e^{max} = 750Nm,$$
$$T_h^{min} = -3000Nm, \qquad T_h^{max} = 0Nm,$$

and the torque rate limits are

$$\Delta T_e \leq \Delta T_e^{limit}, \qquad \Delta T_h \leq \Delta T_h^{limit}, \tag{9}$$

$$\Delta T_e^{limit} = 7500Nm/s,$$
$$\Delta T_h^{limit} = 3000Nm/s,$$

where $i \in \{\text{electric, hydraulic}\}$, ΔT_i (Nm/s) the torque rate, ΔT_i^{limit} (Nm/s) the maximum torque rate limit, T_i^{min} and T_i^{max} (Nm) the minimum and maximum brake torque range respectively. These characteristics of the actuator dynamics will be taken into consideration as constraints of the optimization problem discussed in next section.

3. Model Prediction Control Strategies

In this section we present two MPC strategies which include linear and nonlinear MPC formulations. The proposed algorithms consist of wheel slip control and torque distribution strategies to allocate ABS control torque between HFB and regenerative braking. The first objective is to avoid wheel locking by controlling the wheel slip to a desired slip target, s_{ref} in an emergency situation. Next, the torque delivery is apportioned to the braking actuators while respecting the actuator dynamics and limits. These objectives will be integrated in a single MPC problem which has the advantage of handling multivariable constrained control problems.

For the continuous time system with state x and input u

$$\dot{x} = f(x, u), \tag{10}$$

the equivalent discrete form is

$$x_{k+1} = g(x_k, u_k). \tag{11}$$

Then, the general discrete Optimal Control Problem (OCP) is

$$\min_{x,u} \quad \sum_{k=0}^{N-1} [(x_k - x_{ref})^T Q (x_k - x_{ref}) + (u_k - u_{ref})^T R (u_k - u_{ref})] \tag{12a}$$

$$s.t. \quad x(0) = x_{init}, \tag{12b}$$

$$x_{k+1} = g(x_k, u_k), \quad k = 0, ..., N-1 \tag{12c}$$

$$x^{min} \leq x_k \leq x^{max}, \quad k = 0, ..., N-1 \tag{12d}$$

$$u^{min} \leq u_k \leq u^{max}, \quad k = 0, ..., N-1 \tag{12e}$$

In the above, the objective is to minimize the state and input errors with respect to the given references x_{ref} and u_{ref}, subject to the initial condition, the system dynamics and both the state and input constraints.

In our case we need to find the necessary hydraulic and electric torques on the wheel to achieve the desired longitudinal slip, while at the same time give priority to the use of the electric motor. We choose to neglect the actuator dynamics (6,7) and rather set

$$T_{e_{k+1}} = T_{e_k} + \Delta T_{e_k}, \tag{13}$$

$$T_{h_{k+1}} = T_{h_k} + \Delta T_{h_k}, \tag{14}$$

where we have assumed that the input only changes at times k, $k+1$, ..., $k+N-1$ (with N the prediction horizon). In this way we not only simplify the formulation but we are also given the opportunity to constrain the rate of change of the hydraulic and electric torques, while avoiding setting a target hydraulic and electric torque in the cost function as we demonstrate below. The internal model for the MPC is therefore (1)-(3) augmented with (13)-(14) so that the state and input vectors are $\bar{x} = [V_x \quad \omega \quad T_e \quad T_h]^T$ and $\bar{u} = [\Delta T_e \quad \Delta T_h]^T$. In this work we assume we can measure ω using standard wheel speed sensor in a vehicle and estimate V_x and F_z which are required for the MPC

strategies. Using the augmented system the MPC with sampling time T_s is then

$$\min_{x,u} \quad \sum_{k=0}^{N-1} [q_s(s_{x_k} - s_{ref})^2 + q_T T_{h_k}^2 + q_e \Delta T_{e_k}^2 + q_h \Delta T_{h_k}^2] \tag{15a}$$

$$s.t. \quad \bar{x}(0) = \bar{x}_{init}, \tag{15b}$$

$$\bar{x}_{k+1} = \bar{g}(\bar{x}_k, \bar{u}_k), \quad k = 0, ..., N-1 \tag{15c}$$

$$T_e^{min} \leq T_{e_k} \leq T_e^{max}, \quad k = 0, ..., N-1 \tag{15d}$$

$$T_h^{min} \leq T_{h_k} \leq T_h^{max}, \quad k = 0, ..., N-1 \tag{15e}$$

$$\Delta T_e^{min} \leq \Delta T_{e_k} \leq \Delta T_e^{max}, \quad k = 0, ..., N-1 \tag{15f}$$

$$\Delta T_h^{min} \leq \Delta T_{h_k} \leq \Delta T_h^{max}, \quad k = 0, ..., N-1 \tag{15g}$$

where we choose to penalize the s_x from a given reference through its definition (4), the torque rates ΔT_e and ΔT_h which will force the torques to stabilize to a value, along with an additional weight on the T_h to avoid using the hydraulic brakes when possible and by respecting the constraints from the actuator dynamics. In this way we do not explicitly set references for the electric motor and hydraulic brake torques, but rather leave the MPC to find the optimal values according to the given longitudinal slip reference, the torque and torque rate constraints, and the chosen weights q_s, q_e, q_h, $q_T > 0$. The selection of the weights for both linear and nonlinear MPC strategies in this work are as follows

$$q_s = 0.1 \frac{(\Delta T_e^{limit})^2}{(s_{ref})^2}, \tag{16a}$$

$$q_h = 1000, \tag{16b}$$

$$q_e = 50, \tag{16c}$$

$$q_T = 1 \tag{16d}$$

where we normalize the weight for the slip error according to the torque rate limit and slip reference. Tuning for the weights is by penalizing on the hydraulic brakes and gives priority to the slip reference tracking by using the regenerative braking. The first value of the optimal control input u_1 is applied to the actual system and the optimisation is then repeated for a shifted horizon.

3.1. *Nonlinear MPC*

The internal model employed in the NMPC formulation is based on a discretised version of the wheel dynamics (1-3) found using five steps of the fourth order Runge-Kutta

scheme [31],

$$k_1 = f(x_k, u_k), \tag{17a}$$

$$k_2 = f(x_k + \frac{h}{2}k_1, u_k), \tag{17b}$$

$$k_3 = f(x_k + \frac{h}{2}k_2, u_k), \tag{17c}$$

$$k_4 = f(x_k + hk_3, u_k), \tag{17d}$$

$$x_{k+1} = x_k + \frac{h}{6}(k_1 + 2k_2 + 2k_3 + k_4) \tag{17e}$$

which is then augmented by (13)-(14) like explained above.

In order to solve the NMPC problem in real time the Primal Dual Interior Point (PDIP) method as available in Forces Pro [29] is employed: it has been found that the specific method can provide solutions in real time without the performance degradation associated with a linear MPC formulation or suboptimal NMPC strategies such as the Real Time Iteration (RTI) scheme [30].

3.2. *Linear MPC*

A second method is constructed based on linear MPC to approach the wheel slip control with torque blending strategy problem. This algorithm will be formulated with similar states and inputs as the approach above (section 3) and all constraints remain unchanged. The main difference between the linear MPC and the NMPC is how we define the discrete system dynamics in (13)-(14).

In the linear MPC case, we linearise (1)-(3) about the current values of V_x, ω and the values of T_e, T_h at the previous time step. This allows us to avoid setting target for T_e and T_h as would be the case if we were to linearise about an equilibrium target. If we linearise the continuous system dynamics in (10) about point $(x_{lin}, u_{lin}) = (x_k, u_{k-1})$ we have

$$\dot{x} = Ax + Bu + c, \tag{18}$$

$$\text{where} \qquad c = -(Ax_{lin} + Bu_{lin} - \dot{x}_{lin})$$

Note that $\dot{x}_{lin} \neq 0$ since (x_{lin}, u_{lin}) is not necessarily an equilibrium point and if c is treated as a piecewise constant disturbance the discretised system is then

$$x_{k+1} = A_d x_k + B_d u_k + E c_k \tag{19}$$

where

$$c_k = -(A_d x_k + B_d u_k - x_{k+1})$$

$$A_d = e^{AT_s}, \qquad B_d = \int_0^{T_s} e^{A\eta} d\eta B, \qquad E = \int_0^{T_s} e^{A\eta} d\eta$$

or an approximation can be used for the low T_s used in this work

$$A_d = (I + AT_s), \qquad B_d = T_s B, \qquad E = T_s$$

Then the affine discretised system is

$$x_{k+1} = (I + AT_s)x_k + T_s B u_k + T_s c_k \tag{20}$$

which is then augmented by (13)-(14) as described before. Finally, the Forces Pro solver [29] is employed to solve the linear MPC in real time which can be deployed in a high fidelity vehicle model for simulation which will be explained later in section 5.

4. State Estimation

4.1. *Vehicle Speed Estimation*

Typical sensors that can be found on modern vehicles for the purpose of wheel slip control include wheel angular rate sensors and an accelerometer. However the vehicle speed cannot be reliably measured by a sensor and hence an observer is required to provide its estimation.

In this section we present the vehicle speed estimation needed in the MPC strategies. The vehicle speed is estimated using a Kalman Filter observer with measurements of wheel angular speed ω and longitudinal vehicle acceleration a_x as inputs [26, 28]. In principle, the vehicle speed can be estimated using the average value of wheel speeds during low deceleration, while during high deceleration braking, the longitudinal vehicle acceleration value is used to maintain vehicle speed estimation accuracy. A set of rules is used to adjust the covariance matrices to take into account the high slip ratio values during hard braking and inaccuracies of acceleration measurements at low vehicle speed.

Noise is injected to the wheel speed and acceleration signals in simulation to replicate real vehicle measurements using the Gaussian noise generator in Simulink. Simulation results from a braking on a straight line scenario is illustrated in figure 2 to compare the estimated vehicle velocity and the actual velocity. Figures 2(a)-(b) show the measured signals for wheel speed and acceleration respectively. It can be clearly seen in figure 2(c) that the estimated vehicle velocity converged close to the actual vehicle speed within 400ms.

4.2. *Vertical Tyre Force Estimation*

One important parameter for the internal model of the MPC is the vertical tyre force F_z. In this work we use a simple quasi-static load transfer calculation to capture the dynamics of vertical tyre force in the event of braking

$$\Delta F_z = \frac{mh}{l} a_x, \tag{21}$$

where m, h and l are the vehicle mass, height of CoG and wheelbase respectively. The only input to the estimation calculation is the longitudinal acceleration a_x which can be measured from the accelerometer in the vehicle. The weight shifting between front

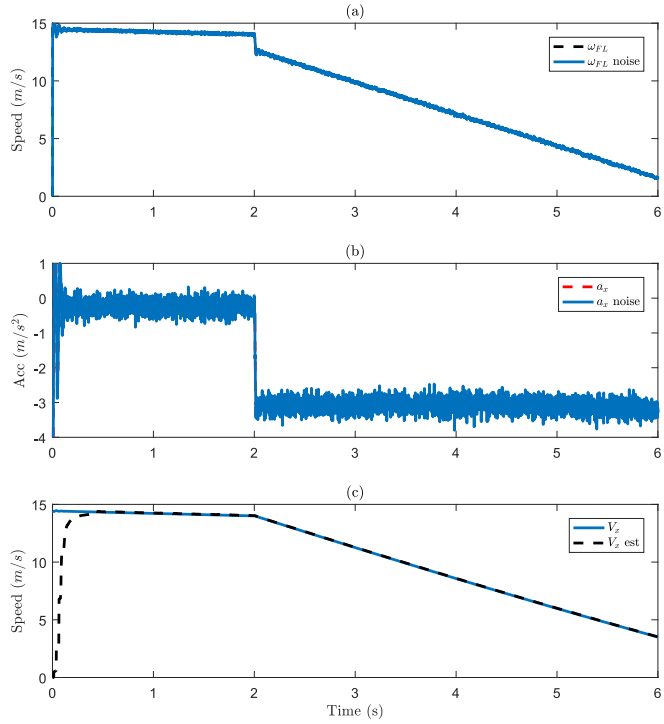

Figure 2. Vehicle speed estimation with noise signal injected.

and rear axle will be updated to the internal model so the MPC can provide accurate torque delivery during slip control operation for better slip reference tracking. Figure 3 shows the wheel slip response during activation of the NMPC controller applied to a high fidelity vehicle simulation model with suspension dynamics. We consider the cases where the dynamic estimate and the static value of normal load are fed to the MPC plant model. Noting that the slip target is set to s_{ref}=-0.1, the inclusion of weight transfer results in considerably better tracking of the slip reference.

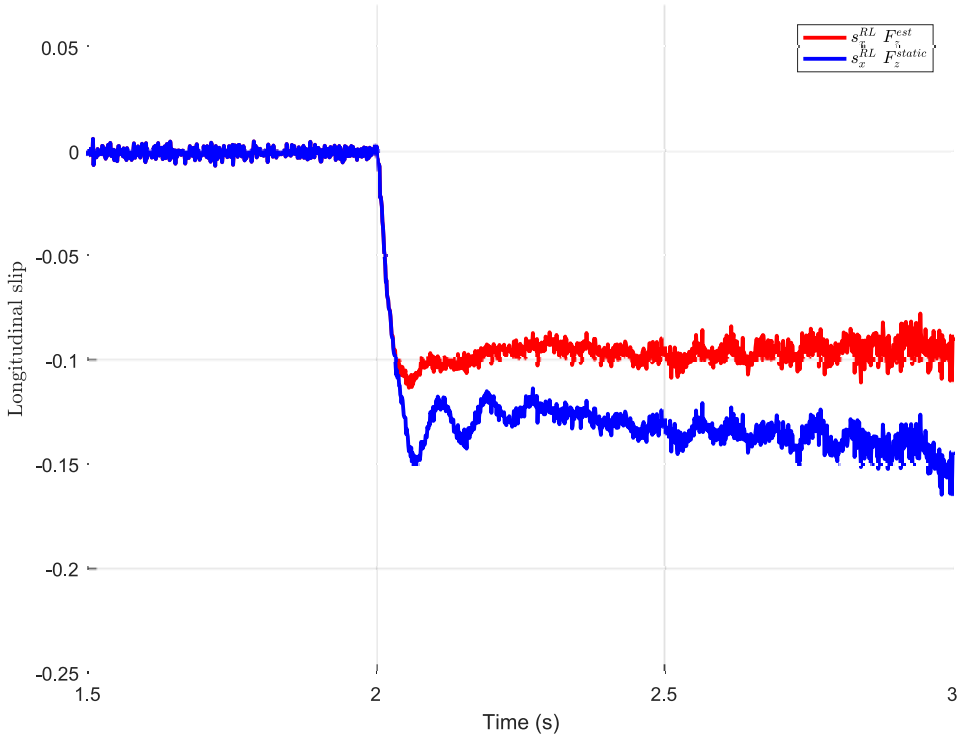

Figure 3. Longitudinal slip with vertical tyre force estimation.

5. Simulation with high fidelity vehicle model

In this section we present the simulation results using the MPC formulations on a high fidelity model. A four wheel drive battery electric vehicle model using four near-wheel motors is constructed in MATLAB/Simulink and IPG CarMaker environment as shown in figure 4. The vehicle's total mass is 1137 kg. A sophisticated driver model in CarMaker is used for closed loop simulation test manoeuvres for consistency.

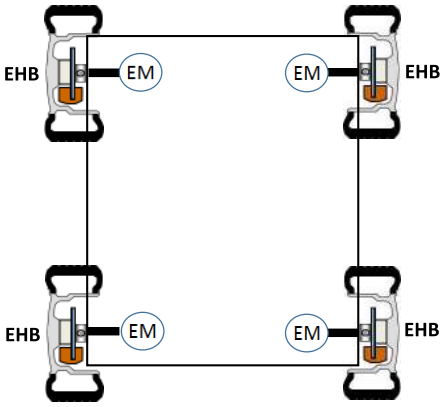

Figure 4. 4WD BEV with 4 EMs.

5.1. *Straight line braking on high μ road*

In this scenario the vehicle initially travels at the speed of 50kph on dry asphalt road (μ=1). The controller is activated at t=2s and the slip target is s_{ref}=-0.1. The vehicle velocity V_x is estimated using the observer presented in section 4.1 considering noise for wheel speed ω and longitudinal acceleration a_x as mentioned in the previous section.

Without slip control hard braking on dry asphalt can lead to locking of the wheels. In the case of the NMPC, the controller manages to bring the wheel slip close to the reference value as illustrated in figures 5(a)-(b). We observe that there is a small undershoot of wheel slips at the front wheels. Since the front electric motors quickly saturate, this can be attributed to the slower friction braking response as seen in figure 5(c).

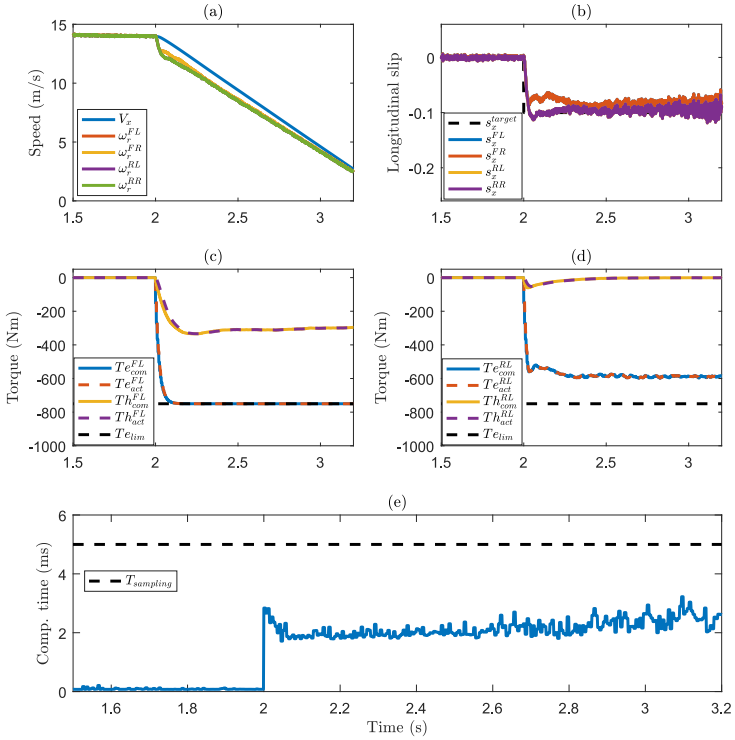

Figure 5. NMPC straight line braking with road μ=1, $V_{initial}$=50kph, s_{ref}=-0.1.

According to figures 5(c)-(d), the brake torque delivered by the EM is insufficient to achieve the desired slip. Consequently, hydraulic brake torque is required to supplement the EM braking torque. It is also worth noting at this point that the commanded torques (T_{com}) from the controller are very close to the actual torques (T_{act}) as delivered by the actuators, a result of including the torque rate constraints in the NMPC formulation.

The manoeuvre is repeated with the linear MPC algorithm to evaluate the controller's performance. Figure 6 indicates that the strategy can be deployed using the linearised internal model for the MPC. The performance is acceptable and comparable to the NMPC approach for most of the duration of the manoeuvre. The linear MPC controller suffers from poor performance at lower speeds as shown in figure 6. Decreasing the sampling time T_s to 1ms, we achieve a more frequent update of the linearisation matrices and the controller performs better at lower V_x as shown in figure 7.

Furthermore we observe, as expected, that the computation time required is smaller for the linear MPC case compared to the NMPC strategy. In figures 5(e) and 6(e) it is shown

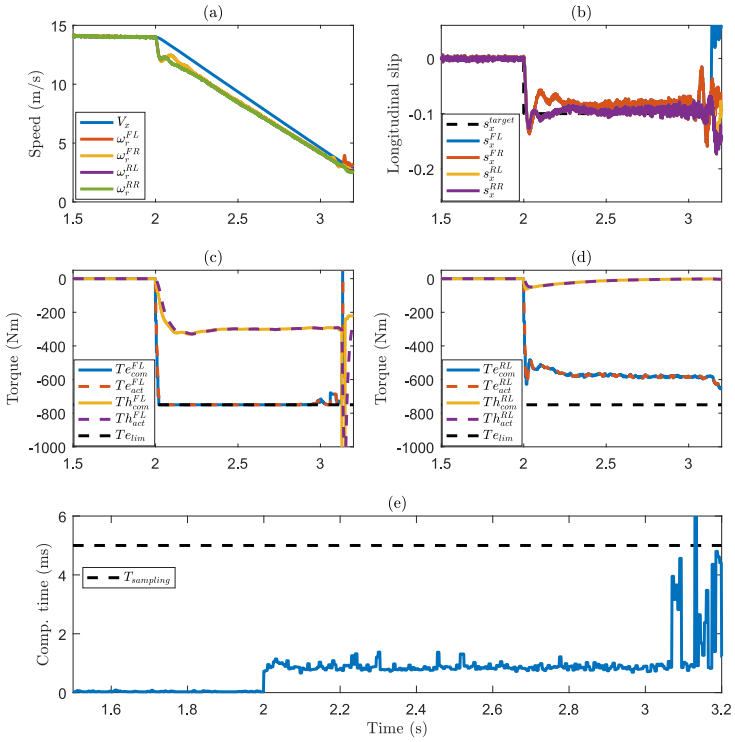

Figure 6. Straight line μ=1 braking for Linear MPC with T_s=5ms.

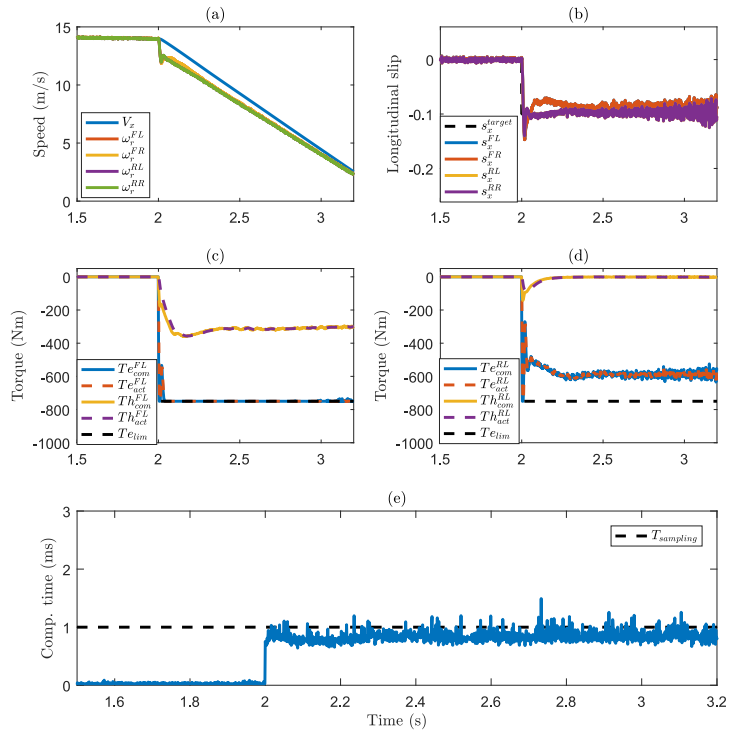

Figure 7. Straight line μ=1 braking for Linear MPC with T_s=1ms.

that a mean time of 1.95ms and 0.99ms are required for NMPC and linear MPC (T_s=5ms) cases respectively for the optimization problem to be solved using a standard desktop (i7-4790M at 3.60GHz with 16GB of memory). That is, in both cases, the computation time is below the 5ms sampling time and hence real time implementation is feasible. However when the T_s is reduced to 1ms to improve the response of the linear MPC at low V_x, there is a risk that the controller cannot be deployed in real time, as illustrated in figure and 7(e).

5.2. *Straight line braking on low μ road*

The next scenario illustrates an emergency braking event with ABS on a packed snow surface (μ=0.3) with initial speed of 50kph. Figures 8(a)-(b) indicate that the slip ratio s_x for individual wheels is well controlled around the reference value s_{ref}=-0.1 using the NMPC algorithm. Results for the linear MPC strategy as shown in figure 9 are acceptable and comparable to the NMPC strategy, except again at low V_x.

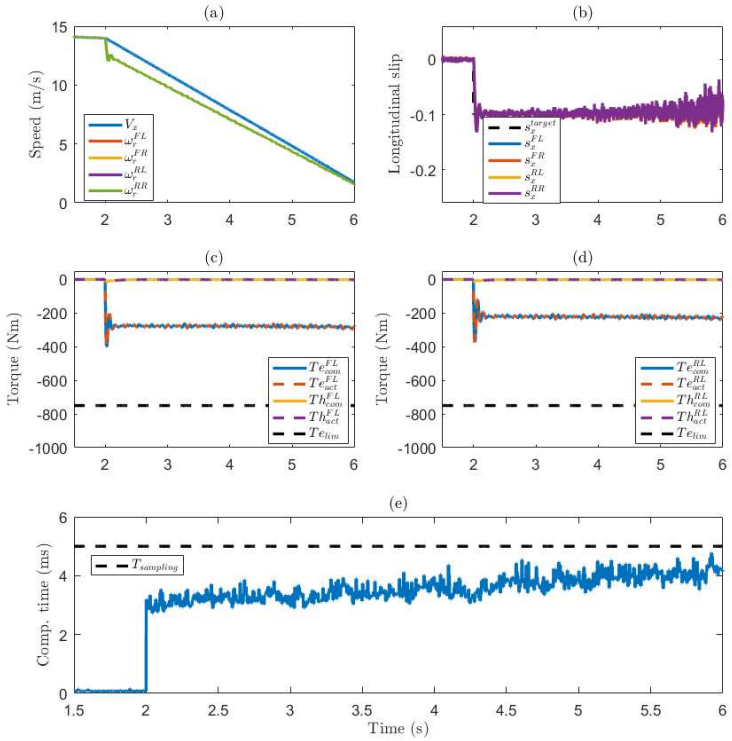

Figure 8. NMPC straight line braking with road μ=0.3, $V_{initial}$=50kph, s_{ref}=-0.1.

A similar observation can be made when T_s is reduced to 1ms where the slip control performance at low V_x is improved as indicated in figure 10. Once again, reducing the sampling time results in a computation time which in places exceeds the sampling time. The mean solve time for the optimization problem is 3.7ms as shown in figure 8(e) for NMPC strategy whereas figure 9(e) indicates 0.92ms is required for the optimization problem to be solved for linear MPC strategy.

In the low μ braking case we observe, as expected, a reduced total torque requirement to achieve the desired slip compared to the high μ case. The proposed MPC strategies are able to prioritise EM braking and in the case of low μ, deliver slip control using solely

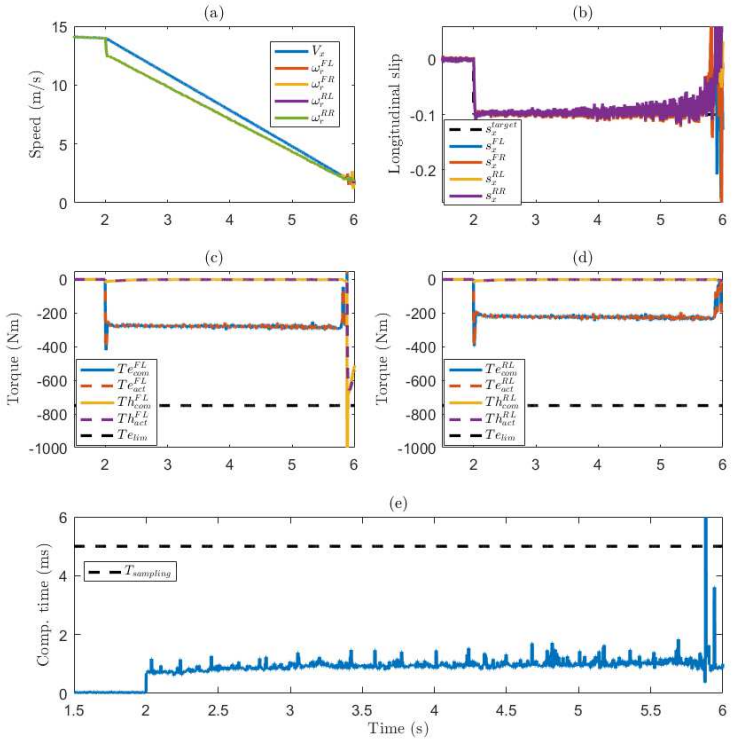

Figure 9. Straight line μ=0.3 braking for Linear MPC with T_s=5ms.

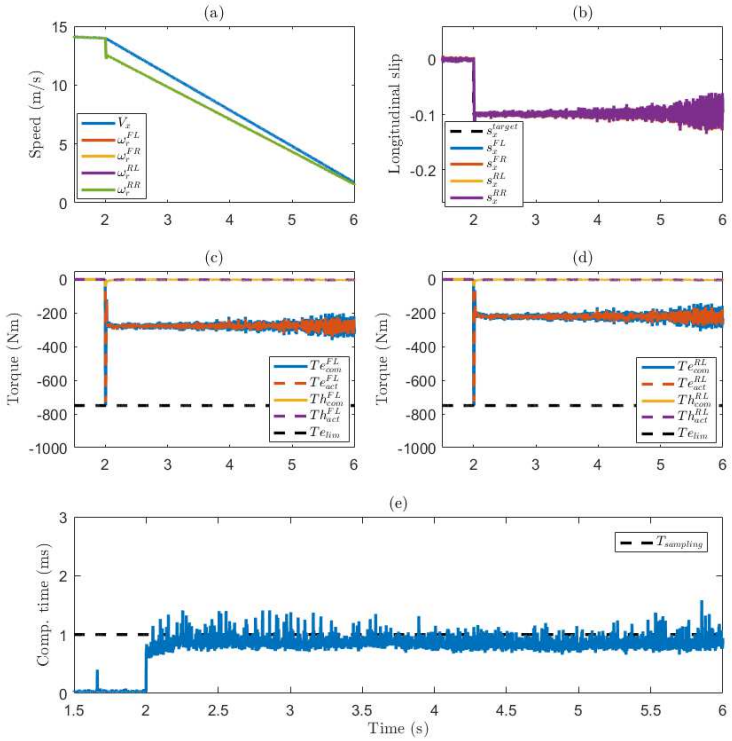

Figure 10. Straight line μ=0.3 braking for Linear MPC with T_s=1ms.

regenerative braking as indicated in figures 8(c)-(d).

5.3. *Straight line braking on split μ road*

Slip control is very important in the presence of uneven friction of road surfaces. In this example, a vehicle is braking on a road with dry asphalt on the left wheels (μ=1) and on snow on the right wheels (μ=0.3) from initial speed of 50kph. A yaw moment is created towards the high friction side of the road if the same brake torque is applied between left and right wheels.

The proposed controller detects the high wheel slip ratio and quickly retards the brake torque to avoid wheel locking and prevent the vehicle from spinning. Lower brake torque is applied to the wheels on the low μ side to maintain the wheel slip within acceptable limits as illustrated in figure 11(a). Figures 11(d)-(g) clearly show the capability of the individual wheel slip control to deliver the required braking torque by either single actuator or both actuators to achieve the reference slip s_{ref}.

Another interesting observation is that the vehicle maintains its steerability and stability for all the wheels for NMPC strategy throughout the braking as evidently indicated by the maximum yaw rate achieved ($\dot{\psi}$=10.1deg/s) and steering wheel angle (δ=73deg) in figure 11(b)-(c). With sufficient countersteering by the CarMaker driver model, the vehicle can be safely stopped. Even without Electronic Stability Control (ESC), the vehicle stability and steering response can be maintained.

Figure 12 shows the performance of the linear MPC strategy for split μ braking. The wheel slip s_x achieved is acceptable during initial braking but becomes unstable towards lower vehicle speeds similar to the straight line braking cases.

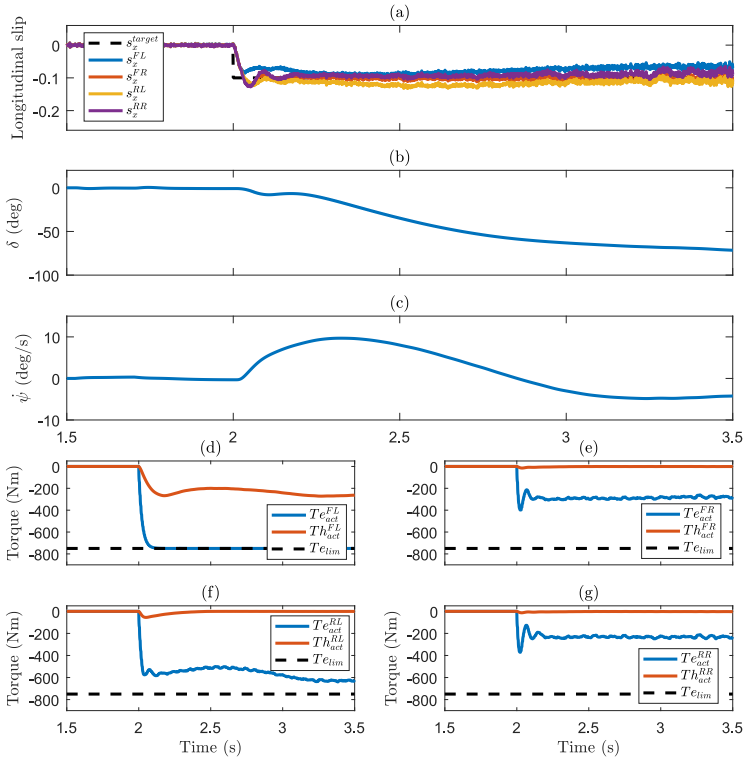

Figure 11. NMPC split μ braking, $V_{initial}$=50kph, s_{ref}=-0.1.

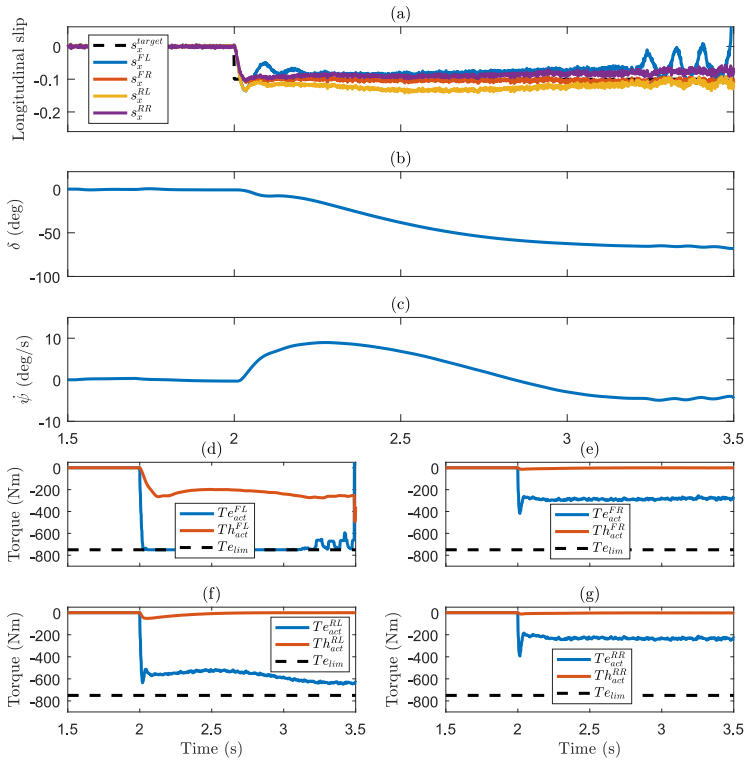

Figure 12. Linear MPC (T_s=5ms) split μ braking.

6. Robustness against tyre-road friction coefficient uncertainty

In the MPC formulation we assume to have information of the road conditions and therefore MF's factor, D used in the internal MPC model which corresponds to the value of the tyre-road μ. In reality we require estimation of road friction coefficient in order to update the D value in the control algorithm. In this section we demonstrate the effect of braking on various type of road friction (μ = 0.3 and 0.9) using a constant D for MF's factor (D=0.6), to study the robustness of the proposed controller.

Figure 13 indicates that the NMPC controller is robust against uncertainties in the tyre-road friction coefficient. In both cases of under-estimation and over-estimation of the μ the controller achieves a stable wheel slip response, however with some notable offset from the reference value. This offset can be avoided with adaptation of the internal model. Even without the adaptation, despite the significant variation in μ, the wheel slip is not excessive and the vehicle can stop safely without any risk of skidding.

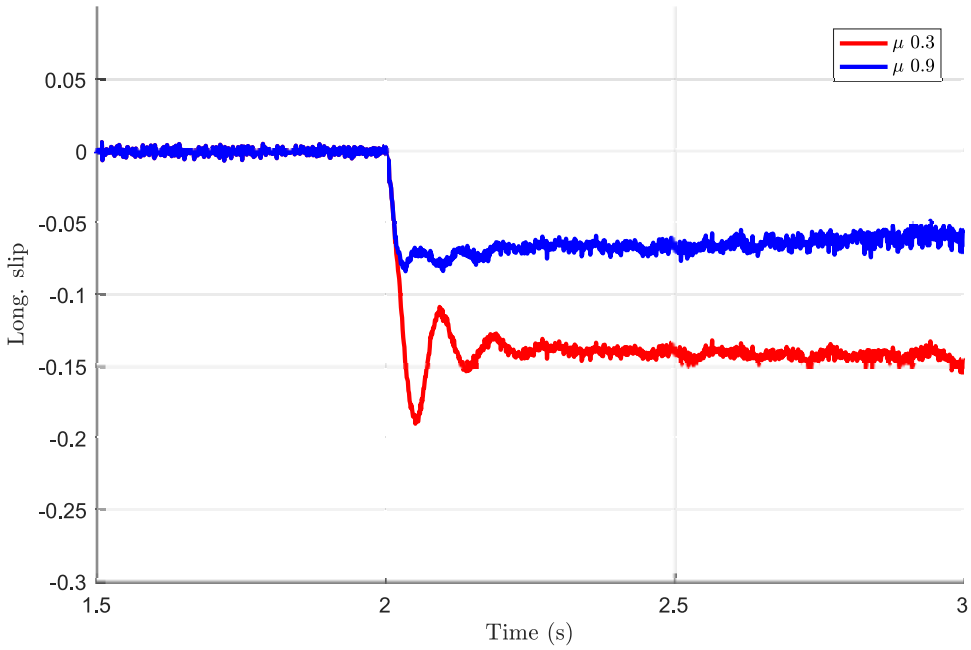

Figure 13. Straight line braking using D_{mpc}=0.6 with μ=0.3 and μ=0.9.

7. Conclusions

In this paper we have demonstrated the design of linear and nonlinear model predictive controllers for the combined wheel slip control and brake torque proportioning between electric motor and friction brake actuators. The implementation of the controllers is complemented with vehicle speed estimation using the available measured variables in a typical modern vehicle. Tyre normal load estimation is also implemented to inform the internal model of the MPC strategies, which, as demonstrated, leads to enhanced wheel slip tracking. The controllers' effectiveness is assessed via simulation using a high fidelity full vehicle dynamic model in a variety of scenarios, including cases of combined longitudinal and lateral dynamics. It is demonstrated that for moderate sampling rates real time implementation of both linear and nonlinear cases is feasible, while achieving high performance in wheel slip tracking for a wide range of speeds. The controllers are also successful in prioritising the use of the electric motor achieving slip control solely by electric braking when the torque demand is within the actuator's capabilities. The linear MPC controller looses performance in slip tracking as the vehicle speed approaches to zero. This drawback in the linear case can be overcome by selecting a smaller sampling rate, which may lead, however, to infeasibility of real time implementation.Finally the controllers demonstrate robustness in the presence of significant tyre-road friction uncertainty in a simulation case study.

References

[1] Chan CC. The State of the Art of Electric, Hybrid, and Fuel Cell Vehicles. Proceedings of the IEEE, 2007;95(4): 704-718.

[2] Chan CC, Wong YS, Bouscayrol A, Chen K. Powering Sustainable Mobility: Roadmaps of Electric, Hybrid, and Fuel Cell Vehicles. Proceedings of the IEEE, 2009;97(4): 603-607.

[3] Crolla D, Cao D. The impact of hybrid and electric powertrains on vehicle dynamics, control systems and energy regeneration. Vehicle System Dynamics 2012;50(1): 95-109.
[4] Heissing B, Ersoy M. Chassis Handbook: fundamentals, driving dynamics, components, mechatronics, perspectives. Wiesbaden: Vieweg+Teubner; 2011.
[5] Kahane JK, Dang JN. The Long-Term Effect of ABS in Passenger Cars and LTVs. NHTSA Technical Report, Washington, USA; 2009.
[6] Tehrani MM, Hairi-Yazdi MR, Haghpanah-Jahromi B, Esfahanian V, Amiri M, Jafari AR. Design of an Anti-Lock Regenerative Braking System for a Series Hybrid Electric Vehicle. Int. J. Automot. Eng. 2011;1(2): 14-27.
[7] Bayar K, Wang J, Rizzoni G. Development of a vehicle stability control strategy for a hybrid electric vehicle equipped with axle motors. Proc. Inst. Mech. Eng. Part J. Automob. Eng. 2012;226(6): 795-814.
[8] Murata S. Innovation by in-wheel-motor drive unit. Vehicle System Dynamics 2012;50(6): 807-830.
[9] De Castro R, Araujo RE, Tanelli M, Savaresi SM, Freitas D. Torque blending and wheel slip control in EVs with in-wheel motors. Vehicle System Dynamics 2012;50(1): 71-94.
[10] Guo JG, Wang JP. Application of Sliding Mode Control for Electric Vehicle Antilock Braking Systems. Adv. Mater. Res. 2012;505: 440-446.
[11] Anwar S. Anti-Lock Braking Control of a Hybrid Brake-By-Wire System. Proc. Inst. Mech. Eng. Part J. Automob. Eng. 2006;220: 1101-1117.
[12] Bera TK, Bhattacharya K, Samantaray AK. Torque blending and wheel slip control in EVs with in-wheel motors. Proc. Inst. Mech. Eng. Part J. Syst. Control Eng. 2011;225(7): 918-934.
[13] Hsiao MH, Lin CH. Antilock braking control of electric vehicles with electric brake. SAE Technical Paper 2005-01-1581; 2005.
[14] Jing H, Liu Z. Wheel Slip Control for Hybrid Braking System of Electric Vehicle. Int Conf on Transp, Mech, and Elec Eng, Changhun, China; 2011.
[15] Velenis E, Katzourakis D, Frazzoli E, Tsiotras P, Happee R. Steady-State Drifting Stabilization of RWD Vehicles. Control Eng Pract. 2011;19(11): 1363-1376.
[16] Gao Y, Chu L, Ehsani M. Design and Control Principles of Hybrid Braking System for EV, HEV and FCV. IEEE Vehicle Power and Propulsion Conference 2007: 384-391.
[17] Wang F, Zhuo B. Regenerative braking strategy for hybrid electric vehicles based on regenerative torque optimization control. Proc. Inst. Mech. Eng. Part J. Automob. Eng. 2008;222(4): 1363-1376.
[18] Chiang W, Yin D, Omae M, Shimuzu H. Integrated Slip-Based Torque Control of Antilock Braking System for In-Wheel Motor Electric Vehicle. IEEJ J. Ind. Appl. 2014;3(4): 318-327.
[19] Mutoh N. Driving and braking torque distribution methods for front- and rear-wheel-independent drive-type electric vehicles on roads with low friction coefficient. IEEE Trans. Ind. Electron. 2012;59(10): 3919-3933.
[20] Basrah MS, Velenis E, Cao D. Four wheel torque blending for slip control in a hybrid electric vehicle with a single electric machine. Int Conf on Sust Energy Eng and App., Bandung, Indonesia; 2015.
[21] Satzger C, De Castro R, Bunte T. A model predictive control allocation approach to hybrid braking of electric vehicles. IEEE Intelligent Vehicles Symposium Proceedings, Dearborn, MI; 2014.
[22] Satzger C, De Castro R. Combined wheel-slip control and torque blending using MPC. International Conference on Connected Vehicles and Expo, Vienna; 2014.
[23] Yuan L, Chen H, Ren B, Zhao H. Model predictive slip control for electric vehicle with four in-wheel motors. Chinese Control Conference, Hangzhou, China; 2015.
[24] Basrah MS, Velenis E, Cao D, Longo S. Integration of torque blending and slip control using realrime nonlinear model predictive control. International Symposium on Advanced Vehicle Control, Munich, Germany; 2016.
[25] Bakker E, Nyborg L, Pacejka HB. Tyre Modelling for Use in Vehicle Dynamics Studies. SAE Technical Paper 870421; 1987.
[26] Savaresi SM, Tanelli M. Active Braking Control Systems Design for Vehicles. London: Springer London; 2010.
[27] Hori Y. Motion control of electric vehicles and prospects of supercapacitors. IEEJ Trans. Electrical and Electronic Eng. 2009;4(2): 231-239.
[28] Kobayashi K, Cheok KC, Watanabe K. Estimation of absolute vehicle speed using fuzzy logic rule-based Kalman filter. Proceedings of American Control Conference. 2005;5: 3086-3090.
[29] Dohamidi A, Jerez J. FORCES Professional. embotech GmbH (http://embotech.com/FORCES-Pro); 2014.
[30] Houska B, Ferreau HS, Diehl M. An auto-generated real-time iteration algorithm for nonlinear mpc in the microsecond range. Automatica. 2011;47(10): 2279-2285.

[31] Press W H, Flannery B P, Teukolsky S A, Vetterling W T. "Runge-Kutta Method" and "Adaptive Step Size Control for Runge-Kutta." ch. 16.1 and 16.2 in Numerical Recipes in FORTRAN: The Art of Scientific Computing, 2nd ed. Cambridge, England: Cambridge University Press, pp. 704-716, 1992.